Int. J. Rock Mech. Min. Sci. & Geomech. Abstr. Vol.30, No.7, pp. 883–899, 1993
Printed in Great Britain

0148-9062/93 $6.00 + 0.00
Pergamon Press Ltd

The Role of Acoustic Emission in the Study of Rock Fracture

D. LOCKNER*

The development of faults and shear fracture systems over a broad range of temperature and pressure and for a variety of rock types involves the growth and interaction of microcracks. Acoustic emission (AE), which is produced by rapid microcrack growth, is a ubiquitous phenomenon associated with brittle fracture and has provided a wealth of information regarding the failure process in rock. This paper reviews the successes and limitations of AE studies as applied to the fracture process in rock with emphasis on our ability to predict rock failure. Application of laboratory AE studies to larger scale problems related to the understanding of earthquake processes is also discussed. In this context, laboratory studies can be divided into the following categories. 1) Simple counting of the number of AE events prior to sample failure shows a correlation between AE rate and inelastic strain rate. Additional sorting of events by amplitude has shown that AE events obey the power law frequency-magnitude relation observed for earthquakes. These cumulative event count techniques are being used in conjunction with damage mechanics models to determine how damage accumulates during loading and to predict failure. 2) A second area of research involves the location of hypocenters of AE source events. This technique requires precise arrival time data of AE signals recorded over an array of sensors that are essentially a miniature seismic net. Analysis of the spatial and temporal variation of event hypocenters has improved our understanding of the progression of microcrack growth and clustering leading to rock failure. Recently, fracture nucleation and growth have been studied under conditions of quasi-static fault propagation by controlling stress to maintain constant AE rate. 3) A third area of study involves the analysis of full waveform data as recorded at receiver sites. One aspect of this research has been to determine fault plane solutions of AE source events from first motion data. These studies show that in addition to pure tensile and double couple events, a significant number of more complex event types occur in the period leading to fault nucleation. 4) P and S wave velocities (including spatial variations) and attenuation have been obtained by artificially generating acoustic pulses which are modified during passage through the sample.

INTRODUCTION

An acoustic emission (AE) is defined as a transient elastic wave generated by the rapid release of energy within a material. It is not surprising that in the geological sciences, significant overlap exists between the studies of AE and seismology. Both disciplines are concerned with the generation and propagation of elastic waves, although at different scales in source dimension and over different frequency ranges. Classical seismology has primarily been interested in seismic radiation from earthquakes greater than magnitude zero, having source dimensions from meters to hundreds of kilometers, and recorded frequencies below a few tens of hertz. Early AE studies in mines [1, 2] were motivated by a desire to predict rock bursts and mine failures. Some of these events are quite large and certainly overlap the range of energy release of microearthquakes currently studied in seismology. In the laboratory, sample dimensions are typically less than a meter and provide a limit to the size of the largest possible fracture events. The most common acoustic emissions studied in the laboratory are controlled by flaws on the scale of the grain size so that most source events are less than a millimeter in dimension. As a result, laboratory studies are generally conducted in the 100 kHz to 2000 kHz range.

Brittle fracture is found to obey similar statistics over source dimensions spanning more than eight orders of magnitude from large crustal earthquakes to laboratory sub-grain-size cracks [3]. For example, the Gutenberg-Richter frequency-magnitude relation for earthquake populations is also observed in laboratory AE studies. This property is discussed in a later section. In addition, laboratory deformation experiments appear

*U.S. Geological Survey, 345 Middlefield Road, MS/977, Menlo Park, California 94025

to exhibit many of the foreshock and aftershock sequences first identified in earthquake studies. Focal mechanisms of AE source events have also been analyzed with some success. Given the similarities between sequences of earthquakes and AE events, a primary goal of laboratory studies has been to investigate the fracture process with the intention of identifying precursory sequences that could be used as earthquake prediction tools. While some progress has been made in this area, this important goal has, for the most part, eluded us. Even so, new studies continue to be reported in which researchers apply more and more sophisticated techniques to the problem of predicting failure. While earthquakes are generally assumed to occur on previously existing faults, the majority of AE studies are conducted on intact laboratory samples. There are a number of reasons that can be used to justify this approach: 1) It is likely that faults heal and strengthen between earthquakes [4, 5]. 2) Natural faults are not smooth and must break through sections of rock where they interlock - in which case laboratory tests would model breaking of these local asperities. 3) Earthquake statistics and AE statistics are similar in many ways. 4) Slip on faults and fracture of intact rock involve the same micromechanical processes [6].

In this paper, I will focus primarily on the recent advances made in the study of rock failure through the use of AE and related techniques. Much of the work in AE has been carried out by metallurgists and in engineering applications such as the detection of flaws in boilers, aircraft and other constructions. These important applications will not be discussed in this review. I will consider contributions made to the field of rock fracture covering approximately the last fifteen years. Three introductory reviews from before this period provide a starting point [7-9]. An additional source of AE research applied to a variety of areas is the series of Pennsylvania State University conferences organized by Hardy and Leighton [10-13].

DISCUSSION

It is well documented that brittle fracture involves the growth of microcracks from stress concentrators such as voids, inclusions and dissimilar grain contacts that result in contrasts of elastic properties [14-18]. This irreversible damage results in both inelastic strain and AE. The acoustic signals that are spontaneously generated from this microcracking provide information about the size, location and deformation mechanisms of the events as well as properties of the medium through which the acoustic waves travel (e.g., velocity, attenuation and scattering).

AE counts, inelastic strain and Omori's law

The simplest detection system, and one that can easily be constructed, involves attaching a piezoelectric transducer to the sample assembly and counting acoustic emissions. Since this technique gives equal weight to all detected events regardless of size, a common modification involves recording peak amplitude and coda length to obtain a rough estimate of the energy radiated by the event. With just a single transducer, however, no corrections can be made for attenuation and radiation pattern of individual events so that energy estimates may not be accurate. Even so, since good correlations have been reported between inelastic strain rate and AE rate [19-23], monitoring AE with a single transducer can be useful in describing damage accumulation rate during a deformation test [24].

The correlation between inelastic strain and AE can be used to relate earthquake aftershock sequences to transient creep behavior in rock. Aftershock sequences have been found to decay with time according to an empirical relation

$$\nu(t) = K/(t+c)^p \tag{1}$$

known as Omori's law. Here K, c and p are constants, and ν is the acoustic emission rate. Omori's law has been used to estimate the probability of damaging aftershocks following large earthquakes [25]. In an unconfined laboratory test on a basalt sample, Hirata [26] analyzed AE bursts that occurred while the sample was held at constant stress (approximately 85% of failure strength). Individual bursts of events were treated as mainshock-aftershock sequences. In this creep experiment, Hirata found that the aftershock sequences underwent a transition from obeying an exponential decay law

$$\nu(t) = K_a \exp\,(-p_a t) \tag{2}$$

to obeying Omori's law with the p-value in Omori's law showing a small decrease as the sample approached failure. Other researchers analyzed the overall AE rate (rather than individual burst sequences) during transient or primary creep in constant stress experiments. Lord and Koerner [27] found that unconfined creep tests on anthracite coal obeyed eq. (1) with $c = 0$ and p decreasing with increasing stress. Lockner and Byerlee [21] conducted creep tests on granite and sandstone samples at 100 MPa confining pressure and stress levels from 45 to 95% of failure strength. They also found a decreasing decay rate with increasing stress level. However, they showed that during transient creep, AE rate obeyed

$$\nu(N) = K_b \exp\,(-qN) \tag{3a}$$

were K_b and q are constants and N is the cumulative number of AE events. Expressed as a function of time this gives

$$\nu(t) = 1/(K_b^{-1} + qt). \tag{3b}$$

For earthquakes, p-values are found to cluster about unity [25]. In this case ($p = 1$) eq. (1) becomes equivalent to eq. (3b). Hirata's first and last decay sequences are replotted in Fig. 1 as functions of time

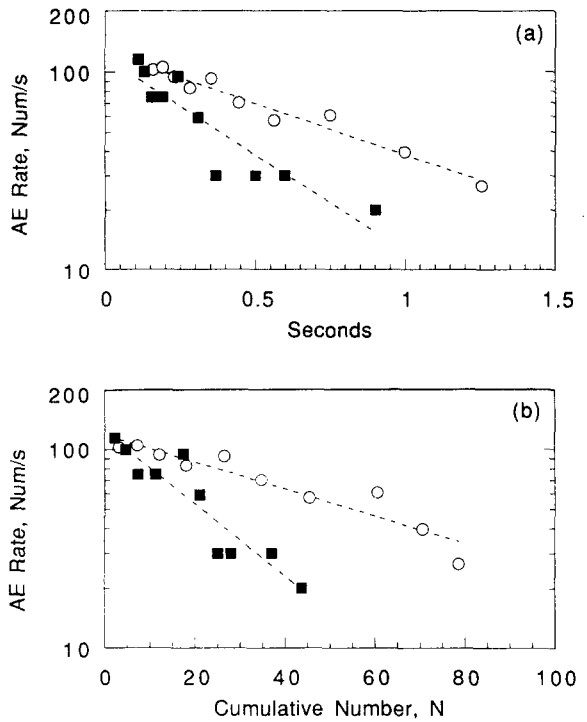

Figure 1. Decay of AE event rate for burst sequences occurring during creep in granite [26]. a) Log (AE rate) plotted *vs.* time; b) Log (AE rate) replotted *vs.* cumulative number of events. Dashed lines show least squares fit to eq. (3) based on transient creep experiments. This function is similar to Omori's law (eq. (1)).

and cumulative number of events, showing that his data are well fit by eq. (3).

I have already mentioned the close correlation observed between inelastic strain and AE. The proportionality depends on such factors as system sensitivity, crack type and attenuation and has been observed to change in a single experiment [23, 28]. If, however, we consider a time interval during which inelastic strain rate remains proportional to AE rate, then eq. (3b) is identical in form to the transient creep rate dependence for rock reported by Lomnitz [29]. This observation is consistent with an aftershock model in which the mainshock raises the stress in the region around its perimeter (due to the stress concentration associated with the propagating fracture [30, 31]). Then the aftershock sequence may be interpreted as a manifestation of the transient creep response which occurs while this surrounding region adjusts to the newly imposed stress state. A similar approach, in which relaxation phenomena are restricted to pre-existing faults, has recently been developed [32]. It should be noted that fluid pressure transients, which may have a dominant influence on aftershock sequences, are not explicitly incorporated in these models.

Amplitudes and the frequency-magnitude relation

In addition to a correlation between AE rate and strain rate, numerous studies have noted a power law frequency-magnitude relation for AE events [26, 33-39]. This corresponds to the well-known Gutenberg-Richter b-value relation for earthquakes

$$\log N(M) = a - b\,M \tag{4}$$

where N is the number of earthquakes greater than magnitude M and a and b are constants. b can vary from one earthquake region to another but is approximately unity.

Different attempts have been made to explain the apparent universality of eq. (4). Evans [40] noted that at a distance r from an elliptical crack the amplitude of a stress wave $\sigma(r,t)$ emitted during the formation of the crack can be related to the tensile stress σ^i_{zz} normal to the crack surface. That is

$$\sigma(r,t) \propto c_1 c_2^2 \sigma^i_{zz} \tag{5}$$

where c_1 and c_2 are respectively the semi-major and semi-minor crack axes. Evans further noted the strong sensitivity of the stress wave amplitude in eq. (5) on crack size. He suggested a probability function of the form

$$\Phi(d) = 1 - \exp[-(d_o/d)^k] \tag{6}$$

would adequately describe the microcrack distribution in a polycrystalline rock. Here $\Phi(d)$ is the probability that a dimension of the grain boundary will exceed d, k is a shape parameter and d_o is a scale parameter. For a transducer whose voltage output V is proportional to the stress wave amplitude and for an average crack dimension $\langle d \rangle$ given by $\langle d \rangle^3 = c_1 c_2^2$, eqs. (5) and (6) can be combined to convert the crack length distribution $\Phi(d)$ to an expected event amplitude distribution

$$\Phi(V) = 1 - \exp[-\alpha(\sigma^i_{zz}/V)^\beta] \tag{7}$$

where α is a constant and $\beta = k/3$. Evans noted that for $V >> (\alpha/2)^{1/\beta}\sigma^i_{zz}$, eq. (7) reduces to

$$\log \Phi(V) = a - \beta \log V \tag{8}$$

($a = \alpha(\sigma^i_{zz})^\beta$) which is equivalent in form to the Gutenberg-Richter eq. (4).

Rather than assuming a microcrack distribution of the form of eq. (6), we can consider actual crack count data. Shown in Fig. 2 are crack density counts from two studies of Westerly granite [18, 41]. Here I have plotted crack density (number/mm^2) in thin section for undeformed samples and for samples loaded to failure. Next, these data sets are combined by taking the difference between the stressed and unstressed densities to represent new cracks added during deformation, and converting from areal crack densities to volumetric densities. By assuming that cracks are approximately disc-shaped ($c_1 \approx c_2 \approx d$), a cumulative crack distribution is plotted in Fig. 3a. The dashed line shows the predicted distribution using eq. (6) with k and d_o selected to fit the two longest crack-length values ($k = 7.2$ and $d_o = 50$ μm). Eq. (6) predicts a more abrupt change in slope at the cross-over crack length d_o than is observed in the crack count data. In any case the data in

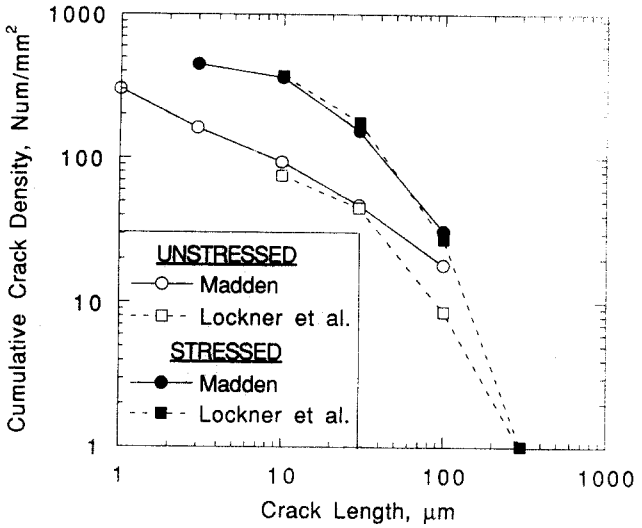

Figure 2. Cumulative crack densities for Westerly granite: open symbols are unstressed samples, closed symbols are stressed to failure; circles are from [41] and squares from [18].

Fig. 3a can be taken as representative of the cumulative microcrack damage occurring in Westerly granite when loaded to failure at 50 MPa confining pressure.

Since we have recorded AE during the deformation of samples, including samples that were analyzed to produce some of the data in Fig. 3a [42], we can compare crack densities to located AE events. AE amplitudes have been corrected for $1/r$ geometric spreading (but not for attenuation) and radiation pattern effects have been partially compensated for by averaging the amplitudes recorded at the six receivers. Transducer/preamp bandwidth is approximately 200 to 1500 kHz with main resonance at 800 kHz. Plotted in Fig. 3b is the fre-quency-magnitude distribution for over 26,000 AE events recorded during loading to the point of failure in a Westerly granite sample at the same confining pressure as the samples used in Fig. 3a. The roll off in the distribution at low amplitude is at least partly due to incomplete sampling of these small events. Otherwise, these data can be reasonably fit by eq. (7), and also by eq. (8) if we assume that the low-amplitude roll off is strictly the result of incomplete sampling. The resulting slope is $\beta = 2.6 \pm 0.2$. These AE events were all located by inverting the relative first arrival times at the recording transducers. They represent all of the located events within a volume of 4.1×105 mm^3 chosen from the central region of the sample. As a result an alternate vertical scale, representing events per unit volume, is shown on the right of Fig. 3b. We can now test the relation, already mentioned, that $\beta = k/3$ by scaling the AE amplitudes (e.g., taking $V^{1/3}$) and comparing them directly to the observed crack length data (shown in Fig. 3c). Here the scaled amplitude data have been offset horizontally and vertically so that the largest amplitude events correspond to the largest observed cracks. Both the crack count data and the AE data should be complete for the largest cracks and AE events (*i.e.*, it is unlikely that any of the largest cracks will be overlooked. Similarly, all large AE events will trigger the recording system. Furthermore, the experi-

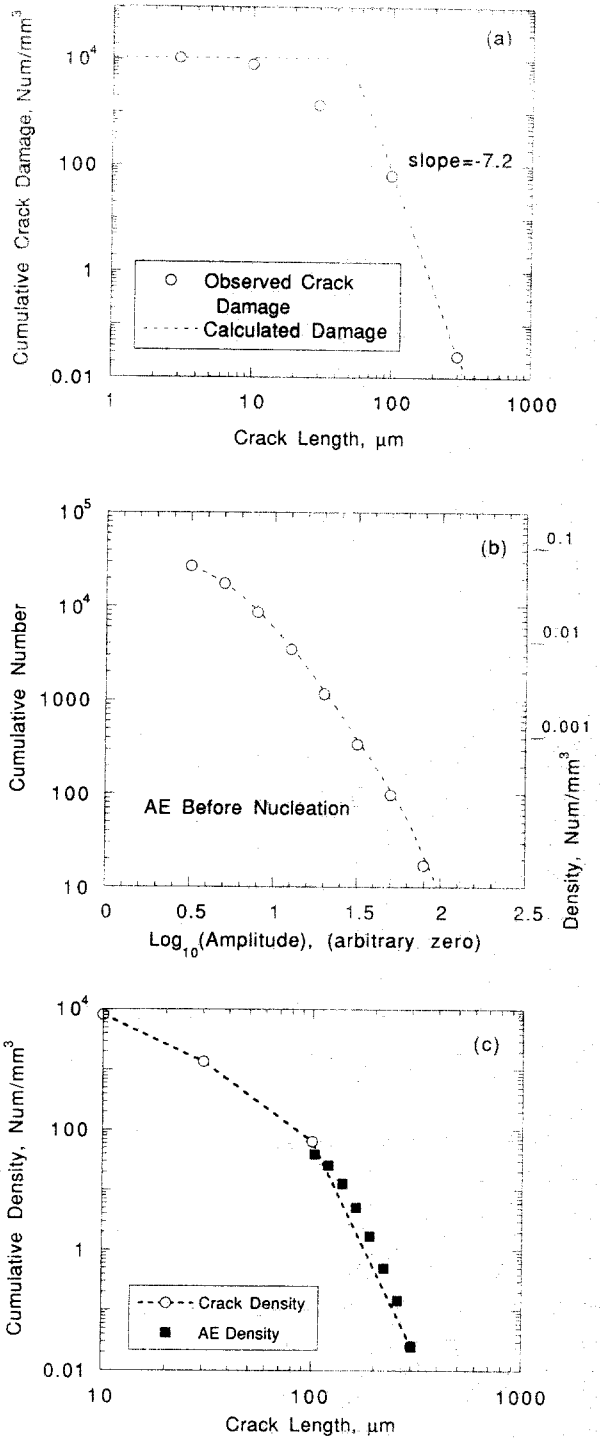

Figure 3. a) Circles: Cumulative microcrack damage due to loading (from data in Fig. 2); line is crack distribution predicted by eq. (6). b) Magnitude-frequency plot for all pre-nucleation AE events occurring in the central region of a Westerly granite sample deformed at 50 MPa confining pressure. Scale on right of plot shows the corresponding AE event density. c) AE events are scaled and replotted so that largest amplitude events correspond to largest microcracks in a sample loaded to failure (see text). AE data had to be shifted vertically by a factor of 600, indicating that the ratio of microcracks to AE events is about 600:1.

ments were designed so that the AE rate was always less than the recording limit of the system.). For these reasons we expect a one to one correspondence between the largest cracks and the largest AE events. Although the AE amplitude data have a limited dynamic range, the slopes of the two data sets are in good agreement and appear to confirm the analysis in eqs. (5) through (8). The horizontal shifting of the amplitude data is allowed since it includes such unknowns as the transducer sensitivity and the event radiation pattern. However, we are not free to shift the amplitude data vertically. The fact that the number of AE events had to be multiplied by a factor of 600 to match the crack count data indicates that less than 0.2% of the new microcracks were accompanied by detectable AE. It would appear that most of the large, grain-size microcracks that formed during loading were inefficient at radiating acoustic energy in the detection bandwidth (possibly because they grew too slowly). This is an important result that has implications for many of the findings discussed in this review. For example, a number of studies have analyzed focal mechanisms of AE events. The question should be asked as to how representative these events are of the total microcrack population.

With regard to the frequency-magnitude relations (eqs. (4) and (8)), numerous laboratory studies, beginning with Mogi [43], have confirmed this general feature of AE amplitude distributions. Most of these studies were motivated by the expectation that changes in b-value would occur prior to failure and therefore could be used for failure prediction. Laboratory studies of AE events consistently show a decrease in b with increasing stress during deformation of intact samples [23, 33, 35, 37]. (Although, a separate article in this issue shows how changes in attenuation can result in apparent b-value changes.) b-value changes were also reported for AE events occurring prior to stick-slip events in a sample containing a sawcut [34]. In this case, foreshocks which occurred during stress buildup had consistently lower b-values than 'background' events, indicating a relative increase of large amplitude AE events prior to stick-slip. Meredith *et al.* [37] developed a model based on subcritical crack growth to explain temporal variations in b. This model contains the overall inverse relation between stress level and b-value but also predicts a dependence of b on stress history. This approach is valuable in that it links the variations in b to established physical mechanisms.

One difficulty in the use of b-value to predict failure, as shown by the laboratory data, is that detectable changes in b are generally the result of large changes in stress. This places strong constraints on the short term stress history of the nucleation region of an earthquake. Indeed, prior to failure in many laboratory samples, inelastic deformation occurs at nearly constant stress. In addition, the amount of strain-weakening observed in some rock types prior to failure may be significantly reduced when loaded in a compliant system such as the Earth. In a recent study, for example, Lockner and Byerlee [44] found that pre-failure decreases in b-value were not consistently observed in a series of fracture tests on granite and sandstone samples.

The search for b-value precursors to earthquakes has had a long history. Numerous studies have reported anomalous changes in b prior to large earthquakes (e.g. [36, 45, 46]). At the same time, questions have been raised as to the reliability of the use of b-value variations as a predictive tool. For example, Frohlich and Davis [47] recently compared b-values from four teleseismic catalogs. They confirmed that b-values for foreshock and aftershock sequences were indeed consistently larger than for mainshocks. However, they concluded that this had no physical significance and resulted from the simple act of treating the largest event in the foreshock–mainshock–aftershock sequence separately (and thereby depleting the foreshock–aftershock set of the largest earthquakes). Wyss and Habermann [48] have also looked at b-value and concluded that systematic errors in determining event magnitudes, for example, have led to fictitious changes in b. The usefulness of b as an earthquake predictor remains an area of continued debate.

Kaiser effect

The Kaiser effect is a well known phenomena in metallurgy [49] and laboratory AE studies [17, 24, 50-54]. It refers to the observation that if a sample is subjected to a cyclic stress history, AE will not occur during the loading portion of a cycle until the stress level exceeds the stress in all previous cycles. Thus the Kaiser effect has potential use as an indicator of prior stress conditions and has been studied in the context of estimating the *in situ* stress state in rock [55, 56]. In this regard, we would expect relatively few foreshocks on a fault segment that has undergone repeated earthquakes and therefore repeated stress cycles. More foreshocks would be expected in a region in which new faults are being created. It should be noted that the Kaiser effect does not reliably occur in all rocks, especially in uniaxial tests and at stresses above about 70% of failure strength. For example, Sondergeld and Estey [51] conducted cyclic uniaxial loading of unjacketed Westerly granite samples. They found that AE commenced well below the peak stress attained in earlier stress cycles. Nordlund and Li [53] also performed cyclic uniaxial tests. They found that the Kaiser effect occurred reliably for a coarse-grained granite until the sample was stressed to near the fracture strength. A fine-grained leptite sample, however, produced AE at levels significantly below previous peak stress. This occurred at all stress levels above about 30% of peak stress. Thus, issues regarding stress level, confining pressure, event amplitude detection threshold, grain size, porosity, minerology and time-dependent crack growth must be addressed to fully understand when the Kaiser effect will be present in a rock.

After verifying that the Kaiser effect does reliably occur in a particular rock, it can be used to provide useful

information about irreversible damage. As an example, consider applications in the field of damage mechanics in which a state variable (damage parameter) is defined to represent the state of internal damage that a material has sustained [17, 57]. If the stress-induced damage (microcrack growth) in a rock is irreversible, then it is likely that significant new damage will occur only when the previous stress state is exceeded [24]. This is essentially the rationale for the Kaiser effect and has led Holcomb and Costin [24, 54] to use AE as a technique for probing stress space to determine the magnitude and shape of the damage surface for a rock. Since stress is a tensor quantity and the application of stress is known to create cracks primarily in the direction of maximum compression, a complete damage parameter can also be expected to be a tensor. This fact suggests that it may be possible to use the Kaiser effect to infer a prior stress state within a rock. Holcomb [58] has recently argued, however, that the commonly-used technique of uniaxial loading along various directions to determine stress history will, in general, give erroneous results. Further work is needed to determine what parameters actually determine the onset of AE in these tests.

Locating AE hypocenters from arrival time data

When more than one transducer are attached to a sample, the relative arrival times of acoustic waves at the known transducer locations can be used to estimate source locations. Except for scaling effects due to sample size, source dimension and frequency content, the determination of AE source locations is analogous to earthquake location procedures. In many applications, samples are loaded to failure, in which case the accompanying microcrack damage is anisotropic and will result in an anisotropic velocity field. It is not uncommon, at high deviatoric stress, to develop a P-wave velocity anisotropy of 40 to 50% [28, 42, 59]. Thus it can be important to include this effect in calculating travel times [42]. If the velocity structure is known, three-dimensional hypocentral determinations require a minimum of four relative arrival times. However, because of the likelihood of timing errors and resolution problems related to station placement, it is highly desirable to have additional arrivals. To attain a location accuracy of about 2 mm in a rock that has a P-wave velocity on the order of 5 mm/μs (5 km/s), a timing accuracy of a fraction of a microsecond is required. As a result, transducers need a frequency response in the megahertz range.

While AE was being used to study rock bursts in mines in the 1940's [27], 3D location studies of rock failure in the laboratory lagged by about 20 years. In an early laboratory 3D location study [60], AE waveforms were recorded as a granite sample was loaded uniaxially to failure. In this case, 22 selected event locations were reported. Now, with improved electronics and automated data collection systems, a single experiment will result in over a thousand times as many locations (Fig. 3b). Part of the appeal of using AE experiments as an analog for earthquakes was that twenty years ago earthquake catalogs could not compete with the large numbers of events recorded in laboratory experiments. Today, however, the quality of seismic catalogs has improved, both in terms of completeness and number of earthquakes, to where this is no longer such an advantage for laboratory experiments. What remains a decided advantage is the ability to precisely control stress, strain, rock type and other parameters.

A typical acoustic-emission-acquisition system for laboratory use involves six or more input channels with preamplifiers near the sample to reduce noise levels. Once the system is armed and ready to record an event, a threshold detector is used to flag the arrival of a potential acoustic signal. If high-speed digitizers are used, they are generally set to record a time interval beginning somewhat before the trigger. In this way, the first arrival of the acoustic wave is captured even if the recording transducer is closer to the event hypocenter than the triggering transducer. If the full waveform is desired, then the contents of the digitizers must be transferred to disk or other storage device for later analysis. This is generally the slowest step in the recording process and will limit system through-put rates to five or ten events per second. Other recording systems pre-process each channel so that instead of recording full waveforms, information such as first-arrival time, peak amplitude, rise time and coda length are recorded. In this case, through-put rates can be increased to 100 to 1000 events per second and loss of events while the system is in a busy state is a much less serious problem. Even so, as I have discussed earlier, only a small fraction of microcrack events appear to generate AE in the megahertz range. In this context, the experiment shown in Fig. 3b was designed to produce AE at a level below the saturation level of the recording system (about 300 events/s). The disparity between number of microcracks and AE events in this example does not reflect a problem with the recording system; the events simply were not there to record.

In the past, researchers have questioned the use of automated threshold detectors (or P-pickers), claiming that hand-picked first arrivals would be more reliable. The relative merits of automated systems have been discussed [42, 61] and it was shown that location accuracies ($\pm$2 to 4 mm) are comparable to hand-picked events, especially for larger amplitude events. For first motion studies it remains desirable to examine individual waveforms. However, for locating events, the shear numbers (e.g., 10,000 to 100,000 per experiment) demand that event timing be automated. Even when full waveforms are recorded, most studies rely on automated computer algorithms to determine first arrivals.

The question of sampling bias due to automatic first arrival pickers has an interesting parallel in seismology. Lockner and Byerlee [61] analyzed P-wave velocities inferred from arrival time inversions of AE events in laboratory experiments (relative arrival times can be used to solve for velocity as well as event location).

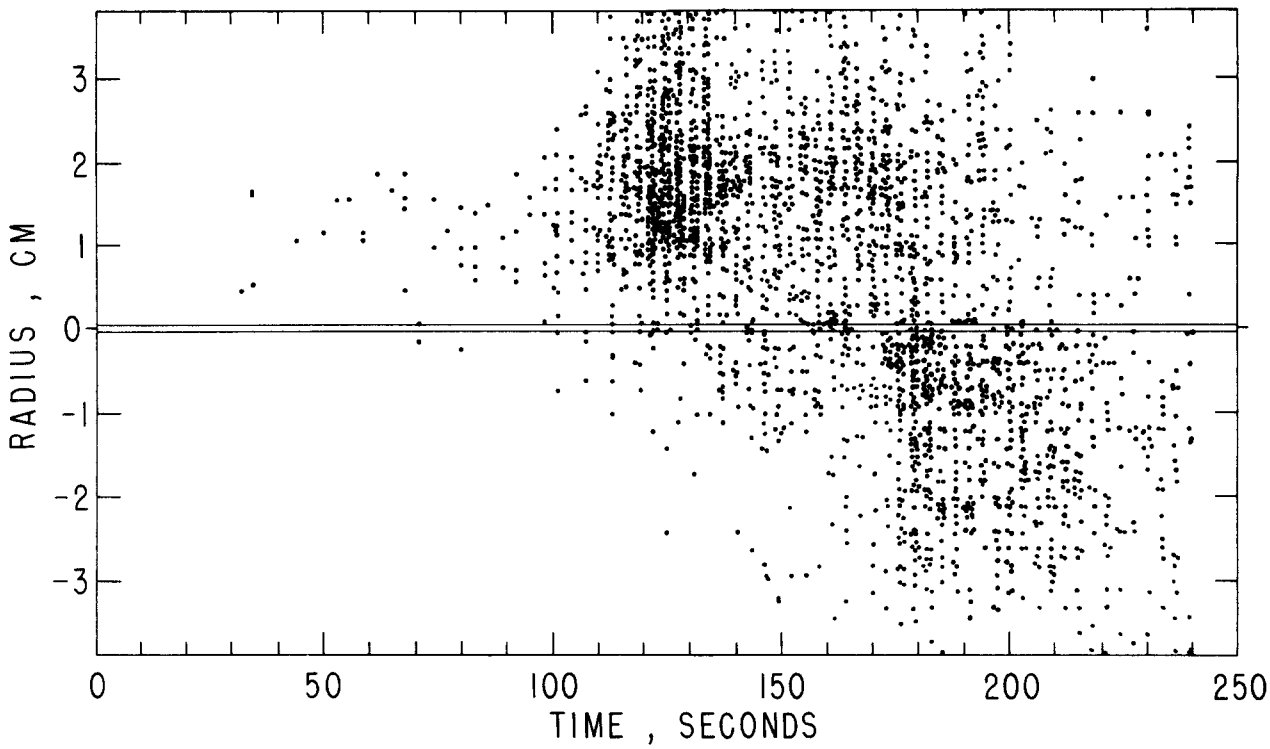

Figure 4. Locations of AE event occurring during hydraulic fracturing of Westerly granite [88]. Horizontal axis is time; vertical axis is cross-section of sample showing injection borehole in center. Dots represent individual AE events and indicate the propagation of the hydrofrac from the borehole to both the top and bottom surface of the sample.

They found that the inversion of small amplitude event data resulted in systematically lower velocity estimates. The problem was that for small events, the P-arrival might be too small to trigger the system so that the later S-arrival would instead be recorded. Thus, there is a tendency, especially for small-amplitude events, to pick the first arrivals late, resulting in a systematic timing error. Similar problems have been identified when small earthquakes were used to search for V_p/V_s anomalies [62], even when events were hand picked.

Hydraulic fracture and fluid-induced shear fracture

AE event locations have been used to study fracture induced by fluid injection. Hydraulic fracturing of boreholes is extensively used to estimate *in situ* stresses as well as to augment flow in geothermal and hydrocarbon reservoir management. During rapid injection of fluid into a borehole, pressure can rise to the point where the wall of the borehole fails in tension and a crack propagates out into the formation. While borehole televiewers, impression packers and other logging tools can determine the orientation of the hydrofrac at the borehole wall, it becomes difficult to know the direction of propagation once the hydrofrac leaves the stress field of the borehole. Lockner and Byerlee [63] demonstrated that AE generated during laboratory hydrofrac experiments in granite could be used to map the orientation of the fracture and infer the propagation rate (Fig. 4). Since that time, similar techniques have been successfully applied in the field to determine hydrofrac orientation [64, 65]. Interestingly, first-motion studies of these microearthquakes indicate that most source mechanisms are double couple shear events and not tensile events [66, 67]. As I will discuss in the section on focal mechanisms, similar results have been found for laboratory AE events.

In addition to tensile failure resulting from rapid injection of fluid into a borehole, a rock mass that is supporting a deviatoric stress below its failure strength may be induced to fail by raising the pore fluid pressure. An increase in fluid pressure P_p in the formation has the effect of reducing the effective stress $\sigma_{\text{eff}} = \sigma - P_p$, but not the deviatoric stress. This effect has many applications in geophysics from induced seismicity (due to reservoir impoundment or fluid injection) to enhanced formation permeability due to development of shear fractures. A number of laboratory studies have used AE source locations to demonstrate the development of fluid-induced failure. In one type of experiment [68] a cylindrical sample of sandstone was held at constant confining pressure (100 MPa) and differential stress (400 MPa). Pore pressure (50 MPa) was then applied to one end of the sample leading to failure after approximately 8 hours. AE locations showed that failure progressed from the end of the sample at high pore pressure down through the sample as a moving fracture front, presumably limited by the rate at which water could diffuse through the sample. This experimental arrangement has recently been repeated for granite [69] at 40 MPa confining pressure with similar results. Acoustic tomography used on the same sample showed a region of increased P-wave velocity, presumably due to filling of dilatant microcracks with pore fluid, moving through the sample.

Lockner and Byerlee [63] tested a different sandstone sample containing an axial borehole at constant confining pressure (100 MPa) and initial differential stress of 400 MPa. In this case, following initial loading, the sample was held at constant axial strain so that as failure progressed, differential stress would decrease. Water was then injected into the borehole at a slow enough rate so that the pore fluid pressure throughout the sample was nearly uniform. As pore fluid pressure increased, reducing the effective confining pressure, the stress state approached the failure envelope for the sandstone and the rock eventually failed along a complex set of fault planes. AE source locations showed a one-to-one correspondence between fault surfaces and AE, allowing the history of faulting to be determined. In a similar geometry, Kranz *et al.* [70] recorded AE during injection and removal of fluid from a borehole in granite samples subjected to hydrostatic as well as deviatoric stress conditions. Focal mechanisms of AE events showed that most events were simple double-couples in nature. These results will be discussed in the section on focal mechanisms.

Fault nucleation and the search for precursors

One of the principal driving forces in using acoustic emission to study rock fracture has been the seemingly endless search for precursory phenomena that could be applied as earthquake prediction tools. While some progress has been made in this regard, the fact that earthquakes are not reliably predicted, especially in the short term, shows the limits of our success in this area. In one sense, we are clearly able to predict failure in the laboratory: once the failure envelope for a rock is determined, failure can be determined from the stress history. Even without knowledge of the failure envelope, increasing strain rate and acoustic emission rate are good indications of approaching failure. These effects do have their counterparts in earthquake prediction. What remains the most reliable prediction tool, and one that is easily believed, is the occurrence of foreshocks. Unfortunately, not all earthquakes have foreshocks, while in other cases, foreshocks are only recognized in retrospect. Why should the precursory phenomena consistently observed in the laboratory be so difficult to observe in the field? The answer appears to be related to the size of the earthquake nucleation zone. In laboratory experiments, the entire sample generally undergoes significant deformation as microcracks grow and cause changes in related physical properties such as modulus, acoustic velocity, attenuation, density, permeability, electrical resistivity, *etc.* Recent observations of moderate earthquakes [71, 72] indicate that the size of the nucleation region responsible for triggering these earthquakes is orders of magnitude smaller that the eventual rupture surface that undergoes coseismic slip. Thus, if a relatively small volume is involved in the accelerating creep phase of an earthquake it may be extremely difficult to detect the associated changes in material properties using remote sensing techniques. This situation may explain the sporadic success of prediction efforts for earthquakes and, on a smaller scale, rockbursts in mines. A related problem that also should be considered is if magnitude 7 earthquakes are simply run-away magnitude 3's, how do we identify the conditions that occur approximately once in 10^4 events that are associated with these run-away events?

Microcrack localization and fault nucleation. I have already commented on the use of *b*-value variations as an indicator of failure in the laboratory and earthquakes in the Earth. Many studies confirm that *b*-values decrease with increasing deviatoric stress. One question that remains unanswered is: Can we expect large precursory changes in deviatoric stress prior to an earthquake? If so, then we would also expect to see significant dilatancy and changes in associated parameters such as velocity and attenuation [42, 59, 69, 73, 74]. Alternatively, as in a creep test, stress may be nearly constant in the final stages of fault nucleation. Under these conditions, laboratory studies do not give consistent results for *b*-value precursors. Recently, there has been considerable interest in fault models showing how large, well-developed faults such as the San Andreas can remain extremely weak due to the presence of high pore fluid pressure [75-78]. If this class of model is correct, then the large changes in deviatoric stress needed to produce the anomalies suggested here might only occur in limited volumes associated with local strong patches, making remote identification difficult.

Faulting can be described as a localization of shear strain in a solid. In this regard, the location of AE sources becomes a powerful tool in imaging the failure process. By contrast, strain and velocity measurements give signals that integrate contributions over volumes that may be much larger than the region of interest. An alternative is to undergo the labor-intensive process of deforming samples and counting cracks using optical and electron microscopy techniques [14, 16, 18, 79-82]. Besides being labor intensive, crack counting has the disadvantage that a single sample cannot be studied at different stages of deformation. Because the recording of AE is essentially passive, it provides an ideal nondestructive method for studying crack growth. Since experiments by Mogi [19] and Scholz [60], numerous AE studies have addressed the question of when in the deformation history of a brittle rock will microcrack localization occur [23, 28, 44, 51, 74, 83-90]. Here I deal specifically with the question of when the macroscopic fracture plane can first be identified from AE locations. The closely related issue of microcrack interaction is addressed later.

A number of studies have reported clustering of AE events from the early stages of loading in deformation experiments. These appear to fall into at least two groups: 1) Tests on heterogeneous samples such as banded sandstones that contain local strength variations [42]. 2) Unconfined samples in which the exposed surface may have been attacked by water vapor (leading to localized stress corrosion) [28, 51, 83]. (Misalignment

of the loading system can also produce non-uniform stresses and early damage localization.) By contrast, homogeneous low-porosity crystalline rocks deformed under jacketed triaxial conditions seem to show much more uniform microcrack accumulation until just before peak stress is reached, or in some cases, after peak stress [42, 44, 86, 88]. For example, source locations for a sample of Westerly granite deformed at 50 MPa confining pressure are plotted in Fig. 5. (This is the same experiment used for Fig. 3b.) In Fig. 5a I have plotted locations of AE events from initial loading to peak stress. Microcrack activity drops off near the ends of the sample due to the lower deviatoric stress in these regions caused by lateral support of the steel endplugs [14]. The central region of the sample, however, shows remarkably uniform microcracking throughout the loading phase of this experiment. By contrast, the nucleation of the fault on the sample surface (Fig. 5c) leads to an abrupt change in the microcracking pattern from uniformly distributed damage accumulation to localized and well-organized microcracking. Lockner *et al.* [42] found that nucleation patch size in Westerly granite was approximately 2000 mm^3.

An earlier creep test on Westerly granite [88] gave similar results. In this case, uniform microcracking occurred throughout the sample during the transient and secondary creep phases, which lasted 2.4 days. Then, in the space of about 300 s, the microcracking localized to a zone which rapidly grew to become the fracture plane. This localization of AE events, which corresponded with an increase in AE rate, was coincident with the onset of accelerating tertiary creep. These experiments represent inelastic strain rates on the order of 10^{-7} to 10^{-9} s^{-1}. The time between the first identifiable clustering of AE and rapid fault propagation represents the fault nucleation phase. For these experiments, this nucleation phase lasted from approximately 500 s for the fastest strain rates to about 10,000 s for the slowest rates. It should be emphasized that Fig. 5 is representative of an end member case in which great care has been taken to eliminate any predisposition to localize the microcracking. That is, the experiment was performed on a confined sample of homogeneous, isotropic, fine-grained granite which was prepared with a uniformly smooth surface and nearly parallel ends (parallel to within 0.03°) to minimize bending moments. A sample that contains pre-existing weakness or variations in material properties will tend to concentrate both stress and damage accumulation. In this case, AE should show spatial clustering from early in the loading cycle and the eventual fault nucleation zone may be identified at low stress.

Microcrack interactions before fault nucleation. The shift from uniform microcracking associated with grain-size or subgrain-size flaws to the growth of a macroscopic fracture represents a jump in scale of flaw size. Thermodynamically, the sample can be thought of as undergoing a phase transition which has led to the application of the concept of self-organized criticality to earthquake processes [91]. An isolated microcrack in an overall compressional stress state cannot grow indefinitely without the continued application of strain energy. Thus macroscopic faulting appears to be the culmination of a process dominated by crack interaction [17, 18, 57, 92-95]. There has been increasing interest in recent years in analyzing the distribution of AE events in terms of spatial and temporal clustering.

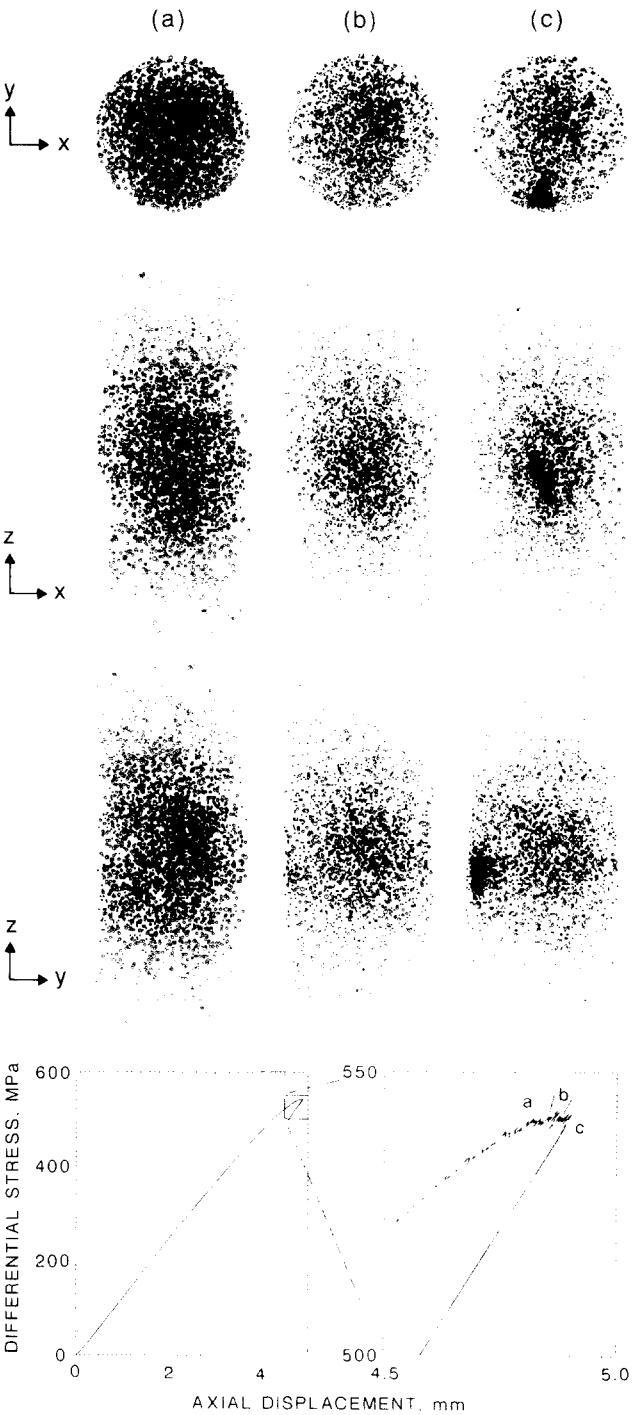

Figure 5. Distribution of AE events in Westerly granite sample at 50 MPa confining pressure. a) Pre-nucleation events, b) pre-nucleation period including peak stress (900 s interval), c) nucleation phase (900 s interval). Middle plots view sample along strike of the eventual fracture plane; lower plots show same events rotated 90°. Stress-displacement curves are shown on right.

Once again, a principal interest has been to identify secular variations in interaction characteristics that would indicate impending sample failure. Lockner *et al.* [18, 44] found that for pre-nucleation events in experiments such as the one shown in Fig. 5, events separated by more than about 5 mm were spatially uncorrelated with each other and occurred randomly throughout the sample. However, events closer than 5 mm did show a consistent degree of correlation. That is, it was about five times as likely for an event to be followed by a second event within a distance of 5 mm as would be expected if the events occurred randomly. Since the stress perturbation around a crack drops off as distance cubed, it is not surprising that the correlation distance for AE events should be comparable to the grain size. It is also important to remember that the correlated events represent less than one percent of the total event population. A similar condition holds for the clustering of earthquakes.

To evaluate the spatial distribution of AE events, I will consider the correlation integral $C(R)$ described by Hirata *et al.* [86] as

$$C(R) = \frac{2}{N(N-1)} N_{(r<R)} \tag{9}$$

for a set of N hypocenters $(p_1, p_2, ..., p_N)$. In this case, $N_{(r<R)}$ is the number of pairs (p_i, p_j) separated by a distance smaller than R. If the distribution has a fractal structure, $C(R)$ is expressed by

$$C(R) \propto R^D \tag{10}$$

were D is a kind of fractal dimension called the correlation exponent [96]. The correlation exponent D can be estimated from the slope of a log-log plot of $C(R)$ versus R (Fig. 6). In this case, the decrease in D corresponds to the change in the spatial distribution of AE events from filling a volume (pre-nucleation) to occurring only on the fault plane (post-nucleation). Thus, if microcracking has organized into a planar feature that is, for example, 20 mm in size, we would expect a slope of 2 in the distance range of 20 mm in Fig. 6. The correlation integral, therefore, is useful in identifying large-scale features in the spatial distribution of events. However, if the early stages of fault nucleation involve only a small cluster of events it may be difficult using the correlation exponent to identify this local change in event distribution when masked by a high level of background activity. Since the human eye is very good at identifying spatial clusters and planar features, the main advantage of using the correlation integral in many cases may be the ability to quantify the degree of clustering.

Hirata *et al.* [86] conducted a creep test on Oshima granite at 40 MPa confining pressure and about 85% fracture strength. They found a systematic decrease in D from 2.75 in transient creep to 2.25 in tertiary creep. Plots of the AE event locations show that this gradual decrease in dimension corresponds to the development of two diffuse clusters in the central region of the sample. The orientation of the eventual fracture plane was not reported and could not be compared to cluster positions. Recently, Lei *et al.* [97] have applied this analysis method to AE locations in a coarse-grained (~5 mm) and fine-grained (<2 mm) granite deformed at 40 and 50 MPa confining pressure and at constant loading rate. The fine-grained Oshima granite again gave $D = 2.7 \pm 0.1$, but in this case with only a slight systematic decrease in the late stages of loading (to D ~2.6). The coarse-grained sample showed nearly constant $D = 2.4 \pm 0.1$ throughout the experiment. Lockner and Byerlee [44] applied this technique to granite and sandstone samples with mixed results. They found $D = 2.7 \pm 0.2$ showed no significant change prior to fault nucleation in the granite sample. In the sandstone sample, however, D gradually dropped from approximately 2.6 to 1.6 over a period of 11 hours. Plots of the locations of AE events during this time interval indicated a gradual process of concentrating and 'focusing' of events in a cluster which formed the nucleation site for the fracture plane. This cluster, while initially diffuse, was identifiable from the initial loading of the sandstone sample.

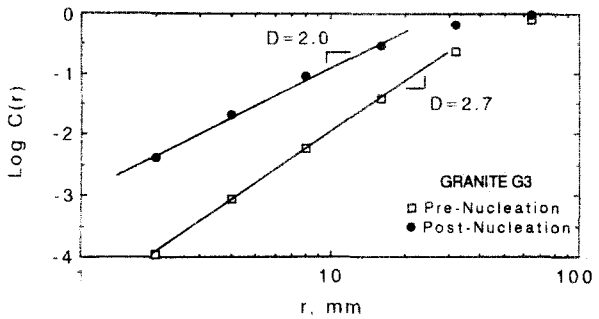

Figure 6. Plot of correlation coefficient showing spatial distribution of AE events before and after fault formation. Slope D represents fractal dimension of event distribution.

A second technique which seemed more useful in visualizing the early organization of microcrack damage into a large-scale feature [44, 86] involves computing a vector for each possible pair of events within a given time interval. Clearly, if all events lie within a plane, then all vectors formed from event pairs will also lie in that plane. An equal-area projection of these vectors provides a sensitive method for identifying the development and orientation of planar features within the AE location data sets.

The preceding discussion has considered the spatial distribution of AE events and the length scale over which they are correlated. It is also important to know how AE events are clustered in time. Omori's law (eq. 1), for example, is a statement of the temporal correlation of aftershock sequences. Nishizawa and Noro [90] have analyzed AE time sequences generated during uniaxial creep experiments in Oshima granite. They fit the time sequences with Poisson and Poisson plus 'self-excitation' functions where self-excitation describes the degree of event interaction. They found that most

events satisfied a Poisson distribution but that a degree of self-excitation did occur (e.g., the occurrence of one event made it more likely that another event would follow). The characteristic interaction time was rather short: between 7 and 42 ms.

Fault propagation

Brittle fracture is commonly accompanied by a sudden loss of strength which, if the loading frame is too compliant, will result in unstable and violent slip. Even for a stiff loading frame, many dense crystalline rocks store sufficient elastic energy to propagate a shear fracture without any externally-supplied energy. Thus final nucleation as well as fault propagation generally involve such high AE rates that individual events cannot be recorded. To solve this problem, Lockner *et al.* [23, 42] developed a feed-back control system in which axial stress was continuously adjusted to maintain constant AE rate. (A similar system was employed by Terada *et al.* [98] but without locating events.) Through the use of this technique, the complete nucleation and growth process of a fault could be observed from the locations of microcrack events (Fig. 7). The left-hand plot shows diffusely spaced AE events in the pre-nucleation stage. Next, the fault nucleates rapidly on the sample surface with the fault orientation clearly observable. The fault then propagates in-plane, expanding as a fracture front of intense AE activity. More detailed analysis of the AE events shows that the fault does not advance smoothly. Rather, there are periods of acceleration and deceleration with different segments of the fracture front advancing rather independently of each other.

Focal mechanisms

With the introduction of multichannel recording systems capable of storing full wave forms, it became practical to conduct first-motion studies of AE events [70, 73, 83, 84, 87, 97, 99, 100]. An example of an AE event recorded at a set of nine transducers, providing good azimuthal coverage, is shown in Fig. 8. As mentioned earlier, thin section studies repeatedly show that microcrack damage in rock loaded in compression is predominantly tensile crack growth parallel to the maximum compressive stress direction [14-16, 18, 82]. In the late stages of fault nucleation, more shearing may be expected as cracks interact and coalesce [18]. However, a commonly sited model for crack coalescence [17, 92, 94] involves buckling of bridges between cracks; a process which should also involve considerable tensile cracking. Thus it was surprising when early results of AE focal mechanisms in granite and andesite [83, 84, 99] indicated that the vast majority of events showed mixed tension and compression first motions consistent with a double-couple mechanism. A pure tensile mechanism, on the other hand, should produce compressive first motions over the entire focal sphere. (Focal mechanism statistics are summarized in Table 1.) In addition, the implied stress axes for these samples appeared strongly misaligned with the applied stress field, indicating significant local stress rotations. Another interesting aspect of these early results was that it seemed possible to construct composite focal mechanisms, suggesting that related AE events occurred either from multiple growth episodes on individual microcracks or from growth of *en echelon* cracks. While these findings were important, the experiments had two potentially important limitations. First, focal mechanisms were poorly constrained since they were determined from only eight or nine transducers. Second, these experiments were all uniaxial and may have been dominated by different crack growth mechanisms than would be possible in a confined experiment.

More recently, confined granite experiments have been conducted [70, 87, 97] which have employed significantly larger transducer arrays (as many as 23 sensors), making the first motion results less ambiguous. In a cyclically loaded experiment, Satoh *et al.* [87] reported results of 215 AE events recorded by 15 or more transducers. They found that about a third of the events had all-compressional first motions (tensile events), 15% satisfied quadrant-type first motions (double couple), while half showed mixed dilatational-compressional first arrivals but could not be fitted by any double couple focal mechanism. I will refer to this last group as 'complex' events. In addition, the relative number of double couple events systematically increased as the sample approached failure. Kranz *et al.* [70] recorded full waveforms during fluid injection into three granite samples. They determined focal mechanisms for a total of 2350 events in these experiments, finding that more than two-thirds of the events were consistent with a double couple mechanism. A quarter of the events were complex and small numbers of both pure compression and pure tension were observed (see Table 1). Pore collapse has been suggested as a mechanism for the pure tensile first motion events. Lei *et al.* [97] have deformed both fine-grained and coarse-grained samples of granite at confining pressures of 40 and 50 MPa. They used a different classification scheme to categorize events which makes it difficult to compare results to earlier experiments. They classified a compressive-first-motion event (due to tensile crack opening) as one for which more than 70% of the observed first motions were compressive (the other studies require 100% compressive motions for this classification). Likewise, a dilatational-first-motion event (e.g., pore collapse) required 70% of the observed first motions to be dilatational. The rest of the events were regarded as shear-type events even though no attempt was made to fit double-couple-type radiation patterns to the individual focal spheres. For the coarse-grained granite, Lei *et al.* found that shear-type events dominated throughout the loading cycle. For the fine-grained Oshima granite, however, dilatational-type events were prevalent below about 30% fracture strength. With the onset of dilatancy, however, compressive-first-motion events dominated, shifting to more shear-type events above about

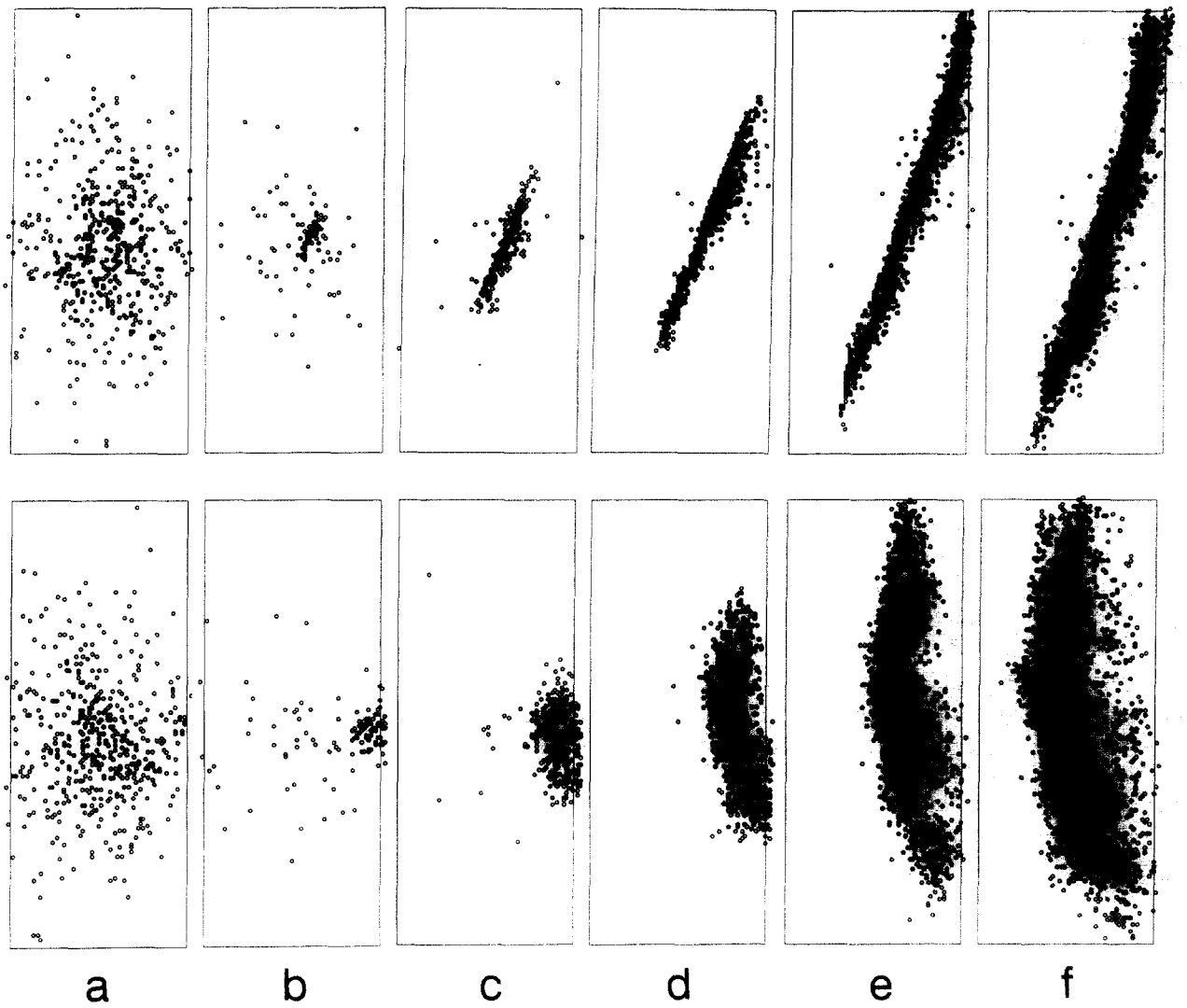

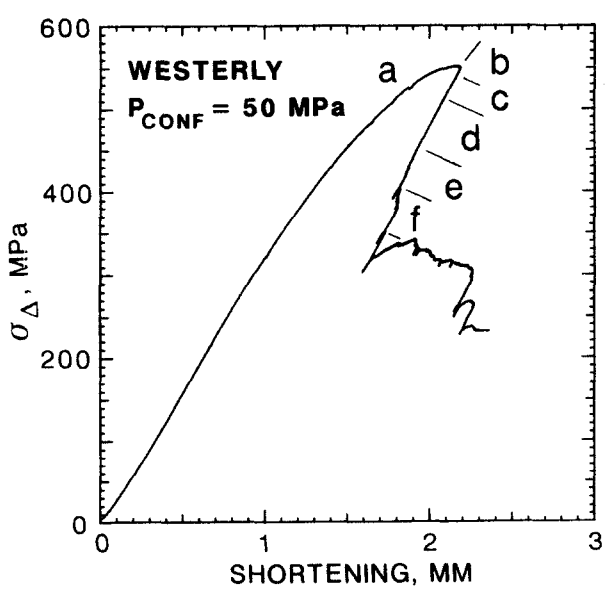

Figure 7. Time sequence of AE events showing the complete fault formation process in a 76.2-mm-diameter sample. a) Pre-nucleation activity, b) fault nucleation, c) to f) fault propagation.

80% fracture strength.

It would appear that we are only beginning to understand the micromechanical source mechanisms responsible for generating AE at megahertz frequencies. The expectation that tensile crack opening would account for the preponderance of detected events has not been borne out. Numerous possibilities exist to explain this fact. I have already shown how detected AE accounts for less than 1% of the total microcrack damage in granite. Thus, detected AE may be the result of an uncommon crack growth process that is not representative of the microcrack populations observed in thin section. For example, Lockner [101] estimated that during secondary creep, subcritical crack growth reduces crack tip stresses so that inelastic deformation is accommodated at an average stress intensity factor less than 60% of the critical stress intensity needed for dynamic crack propagation. A similar result was observed for growth of cracks in glass plates [102]. Since the observed AE is probably the result of unstable crack propagation, the estimate that most cracks are growing stably is consistent with the observed low detection rate for AE events. Furthermore, Yanagidani *et al.* [28] showed a gradual decrease in the number of AE events per unit

Table 1. Summary of AE focal mechanism studies

Study	Conditions	No. of Sensors	Total Events	Relative Percent* D	C	Q	X
Sondergeld & Estey (1982)	uniaxial, granite	8	108	-	-	100	-
Nishizawa *et al.* (1984)	uniaxial, andesite	9	4	-	-	100†	-
Kusunose & Nishizawa (1986)	uniaxial, andesite	9	~16	-	-	100†	-
Satoh *et al.* (1990)	P_{conf} = 40 MPa, cyclic loading, granite	15-20	215	-	36	15	49
Kranz *et al.* (1990)	fluid injection, granite	~20	2350	2	4	69	25
Lei *et al.* (1993)	P_{conf}=40, 50 MPa, granite	23	~1500	~0‡	few percent‡	Q+X=80 to 100‡	

* First motion is: (D) all dilatational (e.g., pore collapse); (C) all compressional (e.g., tensile event); (Q) quadrant type (e.g., double couple); (X) mixed dilatational-compressional but not satisfied by double-couple pattern ('complex').
† Composite solutions.
‡ Estimated values after converting classification scheme (see text).

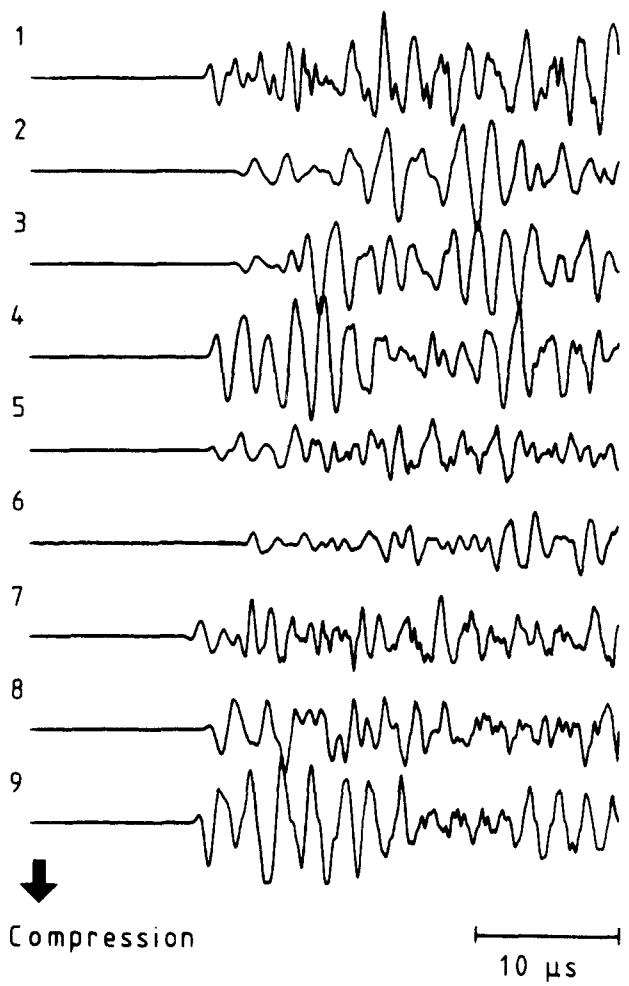

Figure 8. Time traces for AE signals recorded at 9 transducers showing variations in wave forms due in part to source radiation pattern and incidence pattern at receivers (after [28]).

strain during transient and secondary creep. This finding is consistent with the Lockner model [101] in which the average stress intensity at crack tips decreases during creep. Alternatively, tensile crack propagation may be inherently inefficient at generating seismic energy [103]. Finally, at least some models for generating tensile cracks in a compressive ambient stress field (e.g., wing cracks developing at the ends of diagonal flaws [57, 92]) require coupling of shear motion on the main flaw with tensile opening on the crack tips. If the shear motion is coincident with the crack tip extension, the resulting radiation pattern could be quite complex.

Acoustic velocity, attenuation and tomographic studies

While acoustic emission is spontaneously generated in brittle rock, the use of artificial sources is closely related. Piezoelectric transducers function not only as receivers of acoustic signals, but they can also operate as acoustic sources. By measuring the transit time from a known source to an array of known receivers, changes in velocity structure during deformation can be determined [28, 42, 59, 70, 84, 97, 104, 105]. These studies generally assume a homogeneous, although anisotropic velocity field. With the advent of large receiver arrays, tomographic techniques are now used to map heterogeneities in the velocity structure due, for example, to microcracking [73, 74] and fluid penetration [69]. There are numerous studies in which artificial pulsing techniques are used independently to determine velocity and attenuation, without concern for acoustic emissions. Unfortunately, it is beyond the scope of this review to treat these subjects properly.

CONCLUSIONS

Acoustic emission studies continue to provide important information to further our understanding of the brittle fracture process. Physical properties of rocks are often controlled by processes occurring at the grain scale. To understand these processes, observations using optical and electron microscopy are necessary, but require destruction of the sample. Since AE is a natural by-product of brittle fracturing and microcrack growth, analysis of AE signals is well suited to studying these processes. One important impetus for this research has

been to develop methods of predicting failure that could be applied to the problem of earthquake prediction. While this goal has not yet been achieved, significant advances in our understanding of brittle fracture have occurred along the way. The strong correlation between AE activity and inelastic strain has been used to measure damage accumulation in brittle rocks. Significant progress has been made in mapping fault nucleation and propagation through the use of 3D AE event locations. It appears that when preexisting strength heterogeneity exists in a sample, it is likely to control where faulting initiates. In this case, the eventual nucleation site will often appear early in the loading history as a region of increased AE activity. In the absence of preexisting heterogeneity in crystalline rock, microcrack localization leading to fault nucleation occurs late in the loading history; near peak stress in a constant strain rate experiment or at the onset of accelerating tertiary creep in a constant stress experiment. The linear dimension of the fault nucleation region, as indicated by the zone of intense AE activity, is about 8 mm in fine-grained granite and about 30 mm in sandstone with 18% porosity. Once the fault nucleates, it will propagate in-plane as an advancing front of intense microcrack activity. The processes leading to fault nucleation can be much more subtle. Precursory changes in b-value, acoustic velocity and attenuation and microcrack clustering have been reported in many studies. However, many of these effects are the result of large stress or strain excursions. Our inability, at present, to reliably predict earthquakes probably reflects our inability to properly scale these effects observed in the laboratory to dimensions appropriate for crustal earthquakes. With the increasing interest in microearthquakes and the continued investigation of mining problems such as rockbursts, we can expect to see progress in developing appropriate scaling rules.

Acknowledgments. I thank J. Byerlee, T. Hanks and R. Kranz for their many helpful suggestions in preparing this article.

REFERENCES

1. Obert, L. U.S. Bureau of Mines, Rept. Invest. RI-3555, (1941).
2. Obert, L. and Duvall W. U.S. Bureau of Mines, Rept. Invest. RI-3654, (1942).
3. Hanks, T. C. Small earthquakes, tectonic forces. *Science* **256**, 1430–1432 (1992).
4. Blanpied, M. L., Lockner D. A. and Byerlee J. D. Fault stability inferred from granite sliding experiments at hydrothermal conditions. *Geophys. Res. Lett.* **18**, 609–612 (1991).
5. Blanpied, M. L., Lockner D. A. and Byerlee J. D. An earthquake mechanism based on rapid sealing of faults. *Nature* **358**, 574–576 (1992).
6. Lockner, D. A. and Byerlee J. D. How geometric constraints contribute to the weakness of mature faults. *Nature* **363**, 250–252 (1993).
7. Drouillard, T. F. *Acoustic Emission, a Bibliography with Abstracts. Plenum Press*, New York (1979).
8. Liptai, R. G., Harris D. O. and Tatro C. A. (Editors) *Acoustic Emission. ASTM STP 505*, 337 p. Amer. Soc. for Testing and Materials, Philadelphia (1972).
9. Ono, K. (Editor) *Fundamentals of Acoustic Emission.* 349 p. Materials Dept., School of Eng. and Appl. Sci., UCLA, Los Angeles (1979).
10. Hardy, H. R. J. and Leighton F. W. (Editors) *Proceedings First Conference on Acoustic Emission/Microseismic Activity in Geological Structures and Materials.* 489 p. Trans Tech Publications, Clausthal-Zellerfeld, Germany (1977).
11. Hardy, H. R. J. and Leighton F. W. (Editors) *Proceedings Second Conference on Acoustic Emission/Microseismic Activity in Geological Structures and Materials.* 491 p. Trans Tech Publications, Clausthal-Zellerfeld, Germany (1980).
12. Hardy, H. R. J. and Leighton F. W. (Editors) *Proceedings Third Conference on Acoustic Emission/Microseismic Activity in Geological Structures and Materials.* 814 p. Trans Tech Publications, Clausthal-Zellerfeld, Germany (1984).
13. Hardy, H. R. Jr. (Editor) *Proceedings Fourth Conference on Acoustic Emission/Microseismic Activity in Geological Structures and Materials.* 711 p. Trans Tech Publications, Clausthal-Zellerfeld, Germany (1989).
14. Peng, S. and Johnson A. M. Crack growth and faulting in cylindrical specimens of Chelmsford granite. *Int. J. Rock Mech. Min. Sci. & Geomech. Abs.* **9**, 37–86 (1972).
15. Tapponnier, P. and Brace W. F. Development of stress-induced microcracks in Westerly granite. *Int. J. Rock Mech. Min. Sci. & Geomech. Abstr.* **13**, 103–112 (1976).
16. Kranz, R. L. Microcracks in rocks: a review. *Tectonophysics* **100**, 449–480 (1983).
17. Costin, L. S. Deformation and failure. In *Fracture Mechanics of Rock* (Edited by B. K. Atkinson), pp. 167–215. Academic Press, New York (1987).
18. Lockner, D. A., Moore D. E. and Reches Z. Microcrack interaction leading to shear fracture. In *33rd U.S. Rock Mechanics Symposium* (Edited by J. R. Tillerson and W. R. Wawersik), pp. 807–816. Balkema, Rotterdam (1992).
19. Mogi, K. Study of the elastic shocks caused by the fracture of a heterogeneous material and its relation to earthquake phenomena. *Bul. Earthquake Res. Inst.* **40**, 125–173 (1962).
20. Scholz, C. H. Microfracturing and the inelastic deformation of rock in compression. *J. Geophys. Res.* **73**, 1417–1432 (1968).
21. Lockner, D. A. and Byerlee J. D. Acoustic emission and creep in rock at high confining pressure and differential stress. *Bull. of the Seismological Society of Amer.* **67**, 247–258 (1977).
22. Mizutani, H., Yamada I. and Masuda K. Time-dependent properties of rocks and its implications on earthquake prediction. *Earthq. Predict. Res.* **3**, 595–605 (1985).
23. Lockner, D. A., Byerlee J. D., Kuksenko V., Ponomarev A. and Sidorin A. Quasi-static fault growth and shear fracture energy in granite. *Nature* **350**, 39–42 (1991).

24. Holcomb, D. J. and Costin L. S. Detecting damage surfaces in brittle materials using acoustic emissions. *J. Appl. Mech.* **108**, 536–544 (1986).
25. Reasenberg, P. A. and Jones L. M. Earthquake hazard after a mainshock in California. *Science* **243**, 1173–1176 (1989).
26. Hirata, T. Omori's power law aftershock sequences of microfracturing in rock fracture experiment. *J. Geophys. Res.* **92**, 6215–6221 (1987).
27. Lord, A. E. J. and Koerner R. Acoustic emissions in geological materials. In *Fundamentals of Acoustic Emission* (Edited by K. Ono), pp. 261–307. Materials Dept., UCLA, Los Angeles (1978).
28. Yanagidani, T., Ehara S., Nishizawa O., Kusunose K. and Terada M. Localization of dilatancy in Ohshima granite under constant uniaxial stress. *J. Geophys. Res.* **90**, 6840–6858 (1985).
29. Lomnitz, C. Creep measurements in igneous rocks. *J. Geology* **64**, 473–479 (1956).
30. Lawn, B. R. and Wilshaw T. R. *Fracture of brittle solids.* 204 p. Cambridge Univ. Press, (1975).
31. Stein, R., King G. C. P. and Lin J. Change in failure stress on the southern San Andreas fault system caused by the 1992 magnitude = 7.4 Landers earthquake. *Science* **258**, 1328–1332 (1992).
32. Dieterich, J. H. A constitutive law for rate of earthquake production and its application to earthquake clustering. *J. Geophys. Res.*, submitted, (1993).
33. Scholz, C. H. The frequency-magnitude relation of microfracturing in rock and its relation to earthquakes. *Bul. Seismological Soc. Amer.* **58**, 399–415 (1968).
34. Weeks, J. D., Lockner D. A. and Byerlee J. D. Changes in b-value during movement on cut surfaces in granite. *Bull. of the Seismological Society of Amer.* **68**, 333–341 (1978).
35. Cai, D., Fang Y., Sui W., Zhang L., Li J. and Geng N. The b-value of acoustic emission during the complete proces of rock fracture. *Acta Seismologica Sinica* **2**, 129–134 (1988).
36. Imoto, M. and Ishiguro M. A Bayesian approach to the detection of changes in the magnitude-frequency relation of earthquakes. *J. Phys. Earth* **34**, 441–455 (1986).
37. Meredith, P. G., Main I. G. and Jones C. Temporal variations in seismicity during quasi-static and dynamic rock failure. *Tectonophysics* **175**, 249–268 (1990).
38. Zhaoyong, X., Naiguang G. and Shirong M. Acoustic emission m-values of rock failure and mechanic properties of the rock. *J. Seismological Res.* **13**, 291–297 (1990).
39. Sammonds, P. R., Meredith P. G. and Main I. G. Role of pore fluids in the generation of seismic precursors to shear fracture. *Nature* **359**, 228–230 (1992).
40. Evans, A. G. Acoustic emission sources in brittle solids. In *Fundamentals of Acoustic Emission* (Edited by K. Ono), pp. 209–227. Materials Dept., UCLA, Los Angeles (1978).
41. Madden, T. R. Microcrack connectivity in rocks: a renormalization group approach to the critical phenomena of conduction and failure in crystalline rocks. *J. Geophys. Res.* **88**, 585–592 (1983).
42. Lockner, D. A., Byerlee J. D., Kuksenko V., Ponomarev A. and Sidorin A. Observations of quasistatic fault growth from acoustic emissions. In *Fault Mechanics and Transport Properties of Rocks* (Edited by B. Evans and T.-f. Wong), pp. 3–31. Academic Press, London (1992).
43. Mogi, K. Magnitude frequency relation for elastic shocks accompanying fractures of various materials and some related problems in earthquakes. *Bul. Earthquake Res. Inst.* **40**, 831–853 (1962).
44. Lockner, D. A. and Byerlee J. D. Precursory AE patterns leading to rock fracture. In *Proceedings, Fifth Conference on Acoustic Emission/Microseismic Activity in Geological Structures and Materials* (Edited by H. R. Hardy), Trans-Tech Publications, Clausthal-Zellerfeld, Germany, in press (1993).
45. Von Seggern, D. A random stress model for seismicity statistics and earthquake prediction. *Geophys. Res. Lett.* **7**, 637–640 (1980).
46. Jin, A. and Aki K. Temporal change in coda Q before the Tangshan earthquake of 1976 and the Haicheng earthquake of 1975. J. Geophys. Res. **91**, 665-673 (1986).
47. Frohlich, C. and Davis S. Teleseismic b Values; or, much ado about 1.0. *J. Geophys. Res.* **98**, 631–644 (1993).
48. Wyss, M. and Habermann R. E. Seismic quiescence at Parkfield: an error in the data. *Nature*, submitted, (1993).
49. Kaiser, J. *An Investigation into the Occurrence of Noises in Tensile Tests or a Study of Acoustic Phenomena in Tensile Tests.* Ph.D Thesis, Tech. Hosch. Munchen, Munich, Germany (1950).
50. Kurita, K. and Fujii N. Stress memory of crystalline rocks in acoustic emission. *Geophys. Res. Lett.* **6**, 9–12 (1979).
51. Sondergeld, C. H. and Estey L. H. Acoustic emission study of microfracturing during the cyclic loading of Westerly granite. *J. Geophys. Res.* **86**, 2915–2924 (1981).
52. Michihiro, K., Fujiwara T. and Yoshioka H. Study on estimating geostresses by the Kaiser effect of AE. In *Proc. 26th U. S. Symp. on Rock Mechanics* (Edited by E. Ashworth), Balkema, Rotterdam (1985).
53. Nordlund, E. and Li C. Acoustic emission and the Kaiser effect in rock materials. In *Proc., 31st U. S. Rock Mechanics Symposium* (Edited by W. A. Hustrulid and G. A. Johnson), pp. 1043–1050. Balkema, Rotterdam (1990).
54. Holcomb, D. J. General theory of the Kaiser effect. *Int. J. Rock Mech. Min. Sci. & Geomech. Abs.*, in press, (1993).
55. Holcomb, D. J. Using acoustic emissions to determine in-situ stress: problems and promise. *Geomechanics, ASME, AMD* **57**, 11–21 (1983).
56. Hayashi, M., Kanagawa T., Hibino S., Matojima M. and Kitahara Y. Detection of anisotropic geostresses trying by acoustic emission, and non-linear rock mechanics on large excavating caverns. In Proc., *4th Congress Internat. Soc. for Rock Mechanicson Rock Mechanics* pp. 212–218. Montreaux, Switzerland (1979).
57. Ashby, M. F. and Sammis C. G. The damage mechanics of brittle solids in compression. *Pure and Appl. Geophys.* **133**, 489–521 (1990).
58. Holcomb, D. J. Observations of the Kaiser effect under

multiaxial stress states: implications for its use in determining in situ stress. *Geophys. Res. Lett.*, submitted, (1993).
59. Lockner, D. A., Walsh J. B. and Byerlee J. D. Changes in seismic velocity and attenuation during deformation of granite. *J. Geophys. Res.* **82**, 5374–5378 (1977).
60. Scholz, C. H. Experimental study of the fracturing process in brittle rocks. *J. Geophys. Res.* **73**, 1447–1454 (1968).
61. Lockner, D. A. and Byerlee J. D. Velocity anomalies: an alternative explanation based on data from laboratory experiments. *Pure and Applied Geophys.* **116**, 765–772 (1978).
62. Lindh, A. G., Lockner D. A. and Lee W. H. K. Velocity anomalies: an alternative explanation. *Bull. of the Seismological Society of Amer.* **68**, 721–734 (1978).
63. Lockner, D. A. and Byerlee J. D. Hydrofracture in Weber sandstone at high confining pressure and differential stress. *J. Geophys. Res.* **82**, 2018–2026 (1977).
64. House, L. Locating microearthquakes induced by hydraulic fracturing in crystalline rock. *Geophys. Res. Lett.* **14**, 919–921 (1987).
65. Fehler, M. and Phillips W. S. Simultaneous inversion for Q and source parameters of microearthquakes accompanying hydroaulic fracturing in granitic rock. *Bul. Seism. Soc. Amer.* **81**, 553–575 (1991).
66. Fehler, M. C. Stress control of seismicity patterns observed during hydraulic fracturing experiments at the Fenton Hill Hot Dry Rock Geothermal Energy Site, New Mexico. *Int. J. Rock Mech. Min. Sci. & Geomech. Abstr.* **26**, 211–219 (1989).
67. Bame, D. and Fehler M. Observations of long period earthquakes accompanying hydraulic fracturing. *Geophys. Res. Lett.* **13**, 149–152 (1986).
68. Byerlee, J. D. and Lockner D. A. Acoustic emission during fluid injection in rock. In *Proceedings, First Conference on Acoustic Emission/Microseismic Activity in Geological Structures and Materials* (Edited by H. R. Hardy and F. W. Leighton), pp. 87–98. Trans Tech Publications, Clausthal–Zellerfeld, Germany (1977).
69. Masuda, K., Nishizawa O., Kusunose K., Satoh T., Takahashi M. and Kranz R. Positive feedback fracture process induced by nonuniform high-pressure water flow in dilatant granite. *J. Geophys. Res.* **95**, 21,583–21,592 (1990).
70. Kranz, R. L., Satoh T., Nishizawa O., Kusunose K., Takahashi M., Masuda K. and Hirata A. Laboratory study of fluid pressure diffusion in rock using acoustic emissions. *J. Geophys. Res.* **95**, 21,593–21,607 (1990).
71. Johnston, M. J. S., Linde A. T., Gladwin M. T. and Borcherdt R. D. Fault failure with moderate earthquakes. *Tectonophysics* **144**, 189–206 (1987).
72. Linde, A. T. and Johnston M. J. S. Source parameters of the October 1, 1987 Whittier Narrows earthquake from crustal deformation data. *J. Geophys. Res.* **94**, 9633–9643 (1989).
73. Falls, S. D., Chow T., Young R. and Hutchins D. Acoustic emission analysis and ultrasonic velocity imaging in the study of rock failure. *J. Acoustic Emission* **8**, S166–S169 (1989).
74. Itakura, K., Sato K. and Ogasawara A. Monitoring of AE clustering activity prior to main faulting of stressed rock by acoustic tomography technique. In *Proceedings, Fifth Conference on Acoustic Emission/Microseismic Activity in Geological Structures and Materials* (Edited by H. R. Hardy), Trans-Tech Publications, Clausthal-Zellerfeld, Germany, in press (1993).
75. Byerlee, J. Friction, overpressure and fault normal compression. *Geophys. Res. Lett.* **17**, 2109–2112 (1990).
76. Byerlee, J. D. Model for episodic flow of high pressure water in fault zones before earthquakes. *Geology* **21**, 303–306 (1993).
77. Rice, J. R. Fault stress states, pore pressure distributions, and the weakness of the San Andreas fault. In *Fault Mechanics and Transport Properties of Rocks* (Edited by B. Evans and T.-f. Wong), pp. 475–503. Academic Press, London (1992).
78. Sleep, N. H. and Blanpied M. L. Creep, compaction and the weak rheology of major faults. *Nature* **359**, 687–692 (1992).
79. Hallbauer, D. K., Wagner H. and Cook N. G. W. Some observations concerning the microscopic and mechanical behavior of quartzite specimens in stiff, triaxial compression tests. *Int. J. Rock Mech. Min. Sci.* **10**, 713–726 (1973).
80. Hadley, K. Comparison of calculated and observed crack densities and seismic velocities in Westerly granite. *J. Geophys. Res.* **81**, 3484–3494 (1976).
81. Wong, T.-f. Geometric probability approach to the characterization and analysis of microcracking in rocks. *Mech. of Mat.* **4**, 261–276 (1985).
82. Moore, D. E. and Lockner D. A. The role of microcracking in shear-fracture propagation in granite. *J. Struct. Geol.*, submitted (1993).
83. Nishizawa, O., Onai K. and Kusunose K. Hypocenter distribution and focal mechanism of AE events during two stress stage creep in Yugawara andesite. *Pure Appl. Geophys.* **122**, 36–52 (1984).
84. Kusunose, K. and Nishizawa O. AE gap prior to local fracture of rock under uniaxial compression. *J. Phys. Earth* **34**, S45–S56 (1986).
85. Walsh, J. B. Precursors to rock failure observed in laboratory experiments. In *Proc., 1st International Congress on Rock Bursts and Seismicity in Mines* (Edited by N. C. Gay and E. H. Wainwright), pp. 269–275. SAIMM, Johannesburg (1984).
86. Hirata, T., Satoh T. and Ito K. Fractal structure of spatial distribution of microfracturing in rock. *Geophys. J. R. Astr. Soc.* **90**, 369–374 (1987).
87. Satoh, T., Nishizawa O. and Kusunose K. Fault development in Oshima granite under triaxial compression inferred from hypocenter distribution and focal mechanism of acoustic emission. *Tohoku Geophys. J.* **33**, 241–250 (1990).
88. Lockner, D. A. and Byerlee J. D. Development of fracture planes during creep in granite. In *Proceedings, Second Conference on Acoustic Emission/Microseismic Activity in Geological Structures and Materials* (Edited by H. R. Hardy and W. F. Leighton), pp. 11–25. Trans-Tech Publications, Clausthal-Zellerfeld, Germany (1980).

89. Lockner, D. A. and Byerlee J. D. Acoustic emission and fault formation in rocks. In *Proceedings, First Conference on Acoustic Emission/Microseismic Activity in Geological Structures and Materials* (Edited by H. R. Hardy and W. F. Leighton), pp. 99–107. Trans Tech Publications, Clausthal–Zellerfeld, Germany (1977).
90. Nishizawa, O. and Noro H. A self-exciting process of acoustic emission occurrence in steady creep of granite under uniaxial stress. *Geophys. Res. Lett.* **17**, 1521–1524 (1990).
91. Smalley, R. F. J., Turcotte D. L. and Solla S. A. A Renormalization group approach to the stick-slip behavior of faults. *J. Geophys. Res.* **90**, 1894–1900 (1985).
92. Horii, H. and Nemat-Nasser S. Compression-induced microcrack growth in brittle solids: axial splitting and shear failure. *J. Geophys. Res.* **90**, 3105–3125 (1985).
93. Horii, H. and Nemat-Nasser S. Brittle failure in compression: splitting, faulting and brittle-ductile transition. *Philos. Trans. R. Soc. London, ser. A* **319**, 337–374 (1986).
94. Sammis, C. G. and Ashby M. F. The failure of brittle porous solids under compressive stress states. *Acta metall.* **34**, 511–526 (1986).
95. Du, Y. and Aydin A. Interaction of multiple cracks and formation of echelon crack arrays. *Int. J. Numerical and Analytical Methods in Geomech.* **15**, 205–218 (1991).
96. Grassberger, P. Generalized dimensions of strange attractors. *Phys. Lett.* **97**, 227–230 (1983).
97. Lei, X., Nishizawa O., Kusunose K. and Satoh T. Fractal structure of the hypocenter distributions and focal mechanism solutions of AE in two granites of different grain size. *J. Phys. Earth*, in press (1993).
98. Terada, M., Yanagidani T. and Ehara S. A. E. rate controlled compression test of rocks. In *3rd Conf. on Acoustic Emission/Microseismic Activity in Geol. Structures and Materials* (Edited by H. R. Hardy and W. F. Leighton), pp. 159–171. Trans-Tech. Publications, Clausthal-Zellerfeld, Germany (1984).
99. Sondergeld, C. H. and Estey L. H. Source mechanisms and microfracturing during uniaxial cycling of rock. *Pure Appl. Geophys.* **120**, 151–166 (1982).
100. Sondergeld, C. H., Granryd L. A. and Estey L. H. Acoustic emission during compression testing of rock. In *3rd Conf. on Acoustic Emission/Microseismic Activity in Geol. Structures and Materials* (Edited by H. R. Hardy and W. F. Leighton), pp. 131–145. Trans-Tech. Publications, Clausthal-Zellerfeld, Germany (1984).
101. Lockner, D. A. Room temperature creep in saturated granite. *J. Geophys. Res.* **98**, 475–487 (1993).
102. Byerlee, J. D. and Peselnick L. Elastic shocks and earthquakes. *Naturwissenschaften* **57**, 82–85 (1970).
103. Bohler, F. M. and Spetzler H. Radiated seismic energy and strain energy release in laboratory dynamic tensile fracuture. *Pure Appl. Geophys.* **124**, 759–772 (1986).
104. Soga, N., Mizutani H., Spetzler H. and Martin R. J. The effect of dilatancy on velocity anisotropy in Westerly granite. *J. Geophys. Res.* **83**, 4451–4458 (1978).
105. Spetzler, H., Sobolev G., Sondergeld C., Salov B., Getting I. and Koltsov A. Surface deformation, crack formation, and acoustic velocity changes in pyrophyllite under polyaxial loading. *J. Geophys. Res.* **86**, 1070–1080 (1981).